JOURNAL OF SOLID STATE CHEMISTRY 112, 82–91 (1994)

Synthesis, Crystal Structure, and Magnetic Study of $Na_7Sr_2Fe_7F_{32}$

A. Hemon-Ribaud, J. M. Greneche,* and G. Courbion

*Laboratoire des Fluorures (U.R.A. CNRS 449) and *Equipe de Physique de l'Etat Condensé (U.R.A. CNRS 807), Faculté des Sciences, Université du Maine, 72017 Le Mans Cedex, France*

Received July 21, 1993; in revised form November 3, 1993; accepted November 5, 1993

$Na_7Sr_2Fe_7F_{32}$ is orthorhombic (space group *Fddd*) with a = 10.372(3) Å, b = 10.805(3) Å, c = 44.98(2) Å, and Z = 8. The structure was determined from single-crystal data using 1261 independent X-ray reflections, with reliability $R = 0.036$ ($R_w = 0.029$). Corner-sharing iron octahedra give rise to a three-dimensional network $|Fe_7F_{32}|_n^{11n-}$, where linear *trans* connected $|FeF_5|_n^{2n-}$ chains and $|Fe_5F_{26}|^{11-}$ octahedra pentamers can be distinguished. $Na_7Sr_2Fe_7F_{32}$ clearly exhibits an atypic magnetic behavior evidenced from Mössbauer and magnetic measurements ($T_c \approx 35$ K). A competition between ferromagnetic and antiferromagnetic couplings is suggested in relation to a frustrated octahedra network.

INTRODUCTION

In recent years, the investigation of ternary systems $NaF–SrF_2–MF_3$ ($M = Al^{3+}$ or first-row-transition cations) by means of the chloride flux method (1, 2) has allowed the synthesis of fluorinated compounds (3–8) with new structural types. For example, with the trivalent iron cation, we have obtained the $NaSrFeF_6$ phase with a new structural $NaMM'F_6$ type (7) and the $NaSrFe_2F_9$ phase (9) of $NaPbFe_2F_9$ type (10). This paper describes the crystal structure and the magnetic behavior of another iron compound with the formulation $Na_7Sr_2Fe_7F_{32}$.

EXPERIMENTAL

Crystals of $Na_7Sr_2Fe_7F_{32}$ were synthetized using a chloride flux method in a platinum crucible under argon atmosphere. The mixture $NaF + SrF_2 + 2FeF_3 + 6NaCl + 7ZnCl_2$ was heated to 650°C and then slowly cooled to room temperature (5°C/hr). Besides $Na_7Sr_2Fe_7F_{32}$ (plate habit) crystals, $NaFeF_4$ (needle habit) and $Na_5Fe_3F_{14}$ crystals were detected.

A powder sample was prepared in the solid state from a stoichiometric mixture of the elementary fluorides, heated to 575°C in a sealed gold tube and then cooled (30°C/hr) (powder data have been sent to JCPDS).

The thermal study of crushed crystals and powder sample (DTA Netsch 404S) shows a congruent melting point at 620(3)°C.

The magnetic study was performed on a Faraday balance in the temperature range 4.2–300 K for susceptibility measurements and with a Foner and SQUID magnetometer for magnetization experiments in the temperature range 2–105 K.

The Mössbauer study was undertaken in transmission geometry, using a constant acceleration signal transducer and a ^{57}Co source diffused into a rhodium matrix. The sample consists of a mixture of $Na_7Sr_2Fe_7F_{32}$ polycrystalline powder and boron nitride. The first experiments were carried out in a bath cryostat, where the temperature accuracy was estimated at 0.5 K.

STRUCTURE DETERMINATION

A single crystal of $Na_7Sr_2Fe_7F_{32}$ was selected by optical examination, and X-ray diffraction data were collected on a Siemens AED2 four-circle diffractometer. The crystal cell was obtained from a long-exposure oscillation photograph (automatic search) and the cell parameters were refined from 34 reflections measured in double-step scan at $\pm 2\theta \approx 30°$. The space group *Fddd* was unambiguously deduced from systematic extinction conditions: hkl, $h + k = 2n$, $k + l = 2n$; $0kl$, $k + l = 4n$; $h0l$, $h + l = 4n$; and $hk0$, $h + k = 4n-$. Crystal data and conditions of intensity measurement are reported in Table 1. The scattering factors and anomalous dispersion corrections for all atoms are taken from International Tables for X-ray Crystallography (11).

The structure was solved using the direct method (option TREF) of SHELXS-86 (12) and all refinement calculations were performed using the SHELX-76 program (13). Only the reflections in a limiting sphere resolution of about 1 Å ($2\theta < 45°$) were employed for phase refinement. A first solution, including all the cationic positions and only those of seven fluoride anions, was found. Then successive refinements and difference Fourier maps made possible the location of the other fluorine atoms. The refinement of all atomic coordinates and isotropic thermal

0022-4596/94 $6.00

TABLE 1
Conditions of Data Collection and Crystallographic Characteristics for $Na_7Sr_2Fe_7F_{32}$

Symmetry	Orthorhombic
Space group	*Fddd* (No. 70)
Cell parameters	a = 10.372(3) Å
	b = 10.805(3) Å
	c = 44.98(2) Å
	V = 5041(5) Å^3
	Z = 8
Density	d_{cal} = 3.52
Crystal size (10^{-3} mm^3)	0.8
Radiation	Mo$K\alpha$ (graphite monochromatized)
Aperture (mm)	4 × 4
Scanning mode	$\omega/2\theta$ step scan mode in N steps of $\Delta\omega°$
	$36 \le N \le 42$, $\Delta\omega° = 0.035$
	time per step: 1–4 sec
Data collection range	$3.5° \le 2\theta \le 70°$
Range of measurement	$0 \le h \le 16$
	$-17 \le k \le 17$
	$0 \le l \le 72$
Absorption coefficient	μ = 83.3 cm^{-1}
Absorption correction	Gauss method, t_{min} = 0.45, t_{max} = 0.64
Reflections measured	6106 (two independent sets)
Independent	2598 (R_{av} = 0.029)
Used in refinement	1261 ($F_o > 6\sigma(F_o)$)
Number of refined parameters	115
Weighting scheme	$w = 1.16/[\sigma^2(F) + 10^{-5}F^2]$
Secondary extinction factor	$\varepsilon = 1.3(1) \times 10^{-8}$
Maximum electron density in final Fourier synthesis	0.2 $e^- \cdot$ Å^3 (close to F_7)
Reliability factors	R = 0.036, R_w = 0.029

parameters led to R = 0.064, and then R = 0.036, and R_w = 0.029, when applying anisotropic thermal motion. The final results are reported in Table 2; selected interatomic distances and angles are listed in Table 3. A table specifying the calculated and observed structure factors can be obtained from the authors, on request.

STRUCTURAL DESCRIPTION AND CORRELATIONS

The $Na_7Sr_2Fe_7F_{32}$ structure is based on iron octahedra which share corners to give rise to an original three-dimensional network $[Fe_7F_{32}]_n^{11n-}$ into which the Na^+ and Sr^{2+} ions are inserted. The description of the 3D network can be made in two parts. The first feature, illustrated in Fig. 1, corresponds to the existence of pentamers $[Fe_5F_{26}]^{11-}$ built up from five octahedra $[FeF_6]$ among which the central octahedron $[Fe(1)F_6]$ shares four corners in the same plane with the four octahedra $[Fe(3)F_6]$, as already encountered in $Na_3Sr_4Al_5F_{26}$ (4), whereas in $Na_3Sr_4Cr_5F_{26}$ (8) the same entity leads to a tetrahedron of octahedra. All the pentamers are parallel to the (b, c) plane at four levels: z = 1/8, 3/8, 5/8, 7/8. The second feature is the presence of infinite chains of $[Fe(2)F_6]$ octahedra sharing opposite corners (Fig. 2), which are inserted between the pentamers sheets; the infinite chains run either along the [110] direction at level z = 0, 1/2 or along the [1$\bar{1}$0] direction at level z = 1/4, 3/4. A (001) projection (Fig. 3) of the iron cations network gives a schematic description of the stacking of pentamers and chains, and Fig. 4 shows the connection mode between the $[Fe(3)F_6]$ octahedra of a pentamer and the $[Fe(2)F_6]$ octahedra of chains by sharing corners. An $[Fe(2)F_6]$ octahedron belonging to a file is connected by vertices to two octahedra of two pentamers at different levels.

From Table 3, it can be seen that the $[FeF_6]$ octahedra are distorted but, except for Fe(1), the mean Fe–F distances remain very close to the sum of the ionic radii (14) of hexacoordinated Fe^{3+} (0.645 Å) and dicoordinated F^-

TABLE 2
Atomic Parameters, Anisotropic Temperature Factors U_{ij} × 10^4 and B_{eq} (Å^2) for $Na_7Sr_2Fe_7F_{32}$

Atom	Site	x	y	z	U_{11}	U_{22}	U_{33}	U_{23}	U_{13}	U_{12}	B_{eq} (Å^2)
Sr1	16*g*	1/8	1/8	0.27504(2)	127(4)	203(4)	145(4)	0	0	41(4)	1.25(3)
Fe1	8*b*	1/8	1/8	5/8	131(8)	57(7)	62(7)	0	0	0	0.66(6)
Fe2	16*d*	1/2	1/2	1/2	67(5)	73(5)	105(5)	1(4)	6(4)	−1(5)	0.64(4)
Fe3	32*h*	0.1110(1)	0.3615(1)	0.18213(2)	137(4)	66(3)	80(3)	3(3)	−3(3)	19(3)	0.75(3)
Na1	8*a*	1/8	1/8	1/8	383(30)	51(20)	100(22)	0	0	0	1.4(2)
Na2	16*g*	1/8	1/8	0.3793(1)	379(23)	598(28)	175(21)	0	0	238(25)	3.0(2)
Na3	32*h*	0.1226(3)	0.3770(3)	0.3162(1)	468(18)	229(13)	361(14)	−26(13)	84(16)	80(19)	2.8(1)
F1	32*h*	0.0024(4)	0.2780(3)	0.1547(1)	295(20)	257(21)	215(18)	−86(16)	−112(17)	16(19)	2.0(2)
F2	32*h*	0.0680(3)	0.0040(3)	0.0378(1)	216(18)	173(17)	206(18)	93(16)	−12(14)	41(17)	1.6(1)
F3	32*h*	0.1133(4)	0.3910(3)	0.2612(1)	166(18)	226(18)	200(16)	21(15)	26(15)	−110(17)	1.6(1)
F4	32*h*	0.0195(3)	0.0370(3)	0.3012(1)	162(19)	153(17)	300(20)	−30(15)	5(16)	75(15)	1.6(1)
F5	32*h*	0.0119(3)	0.4478(3)	0.0416(1)	148(18)	202(17)	139(17)	51(14)	11(15)	33(16)	1.3(1)
F6	32*h*	0.0008(4)	0.0247(3)	0.8351(1)	209(18)	245(20)	209(18)	14(16)	−85(17)	63(17)	1.7(1)
F7	32*h*	0.1072(7)	0.4968(4)	0.0958(1)	1704(65)	234(22)	208(20)	−163(18)	27(33)	−10(41)	5.6(3)
F8	16*g*	1/8	1/8	0.5081(1)	281(31)	328(31)	247(29)	0	0	−216(30)	2.2(2)
F9	16*e*	0.4478(6)	1/8	1/8	141(32)	659(51)	1889(96)	−3(71)	0	0	7.1(5)

TABLE 3
Main Interatomic Distances (Å) and Angles (°) in $Na_7Sr_2Fe_7F_{32}$

$Fe(1)^{3+}$ octahedron

Fe(1)	F(9)	F(9)	F(7)	F(7)	F(7)	F(7)
F(9)	**1.838(6)**[a]	3.676(8)	2.525(7)	2.781(7)	2.781(7)	2.525(7)
F(9)	180.0(0)	**1.838(6)**[a]	2.781(7)	2.525(7)	2.525(7)	2.781(7)
F(7)	84.5(2)	95.5(2)	**1.918(4)**	2.653(9)	2.795(8)	3.818(8)
F(7)	95.5(2)	84.5(2)	87.5(3)	**1.918(4)**	3.818(8)	2.795(8)
F(7)	95.5(2)	84.5(2)	93.6(3)	168.9(4)	**1.918(4)**	2.653(9)
F(7)	84.5(2)	95.5(2)	168.9(4)	93.6(3)	87.5(3)	**1.918(4)**

⟨Fe(1)–F⟩ = 1.891 Å

$Fe(2)^{3+}$ octahedron

Fe(2)	F(8)	F(8)	F(3)	F(3)	F(5)	F(5)
F(8)	**1.907(1)**	3.815(2)	2.676(4)	2.723(4)	2.763(5)	2.704(4)
F(8)	180.0(0)	**1.907(1)**	2.723(4)	2.676(4)	2.704(4)	2.763(5)
F(3)	89.0(1)	91.0(1)	**1.911(4)**[a]	3.822(5)	2.698(4)	2.773(6)
F(3)	91.0(1)	89.0(1)	180.0(0)	**1.911(4)**[a]	2.771(4)	2.698(5)
F(5)	91.2(2)	88.8(2)	88.4(2)	91.6(2)	**1.958(4)**	3.913(4)
F(5)	88.8(2)	91.2(2)	91.6(2)	88.4(2)	180.0(0)	**1.958(4)**

⟨Fe(2)–F⟩ = 1.925 Å

$Fe(3)^{3+}$ octahedron

Fe(3)	F(6)	F(2)	F(4)	F(1)	F(7)	F(5)
F(6)	**1.893(4)**[a]	2.867(6)	3.785(3)	2.617(6)	2.692(6)	2.710(5)
F(2)	98.4(2)	**1.894(4)**[a]	2.585(5)	2.697(6)	3.841(5)	2.810(5)
F(4)	174.3(1)	86.0(2)	**1.897(4)**[a]	2.826(5)	2.644(7)	2.711(5)
F(1)	87.3(2)	90.6(2)	96.2(2)	**1.899(4)**[a]	2.777(6)	3.896(5)
F(7)	88.7(2)	172.4(2)	86.7(2)	92.2(2)	**1.956(4)**	2.683(6)
F(5)	88.2(1)	92.3(2)	88.1(1)	174.9(2)	85.4(2)	**2.001(4)**

⟨Fe(3)–F⟩ = 1.923 Å

Bridging angles: Fe(2)–F(8)–Fe(2) = 158.0(3) (in files)
Fe(2)–F(5)–Fe(3) = 137.7(2) (file–pentamer)
Fe(1)–F(7)–Fe(3) = 164.5(4) (in pentamers)

$Sr(1)^{2+}$ polyhedron [10]

2 × Sr(1)–F(4) = 2.459(4)
2 × Sr(1)–F(2) = 2.475(4)
2 × Sr(1)–F(3) = 2.610(4)
2 × Sr(1)–F(2) = 2.804(4)
2 × Sr(1)–F(3) = 2.883(3)
⟨Sr(1)–F⟩ = 2.646 Å
$d_{Shannon}$ = 2.67 Å

$Na(1)^{+}$ polyhedron [8]

4 × Na(1)–F(1) = 2.477(4)
4 × Na(1)–F(6) = 2.746(4)
⟨Na(1)–F⟩ = 2.611 Å
$d_{Shannon}$ = 2.49 Å

$Na(2)^{+}$ polyhedron [8]

2 × Na(2)–F(1) = 2.277(5)
2 × Na(2)–F(6) = 2.323(4)
2 × Na(2)–F(9) = 2.811(2)
2 × Na(2)–F(7) = 2.964(7)
⟨Na(2)–F⟩ = 2.594 Å
$d_{Shannon}$ = 2.49 Å

$Na(3)^{+}$ polyhedron [7]

Na(3)–F(4) = 2.202(5)
Na(3)–F(6) = 2.206(5)
Na(3)–F(3) = 2.480(6)
Na(3)–F(1) = 2.490(5)
Na(3)–F(5) = 2.626(5)
Na(3)–F(2) = 2.703(5)
Na(3)–F(9) = 2.758(7)
⟨Na(3)–F⟩ = 2.495 Å
$d_{Shannon}$ = 2.43 Å

[a] Terminal fluorine.

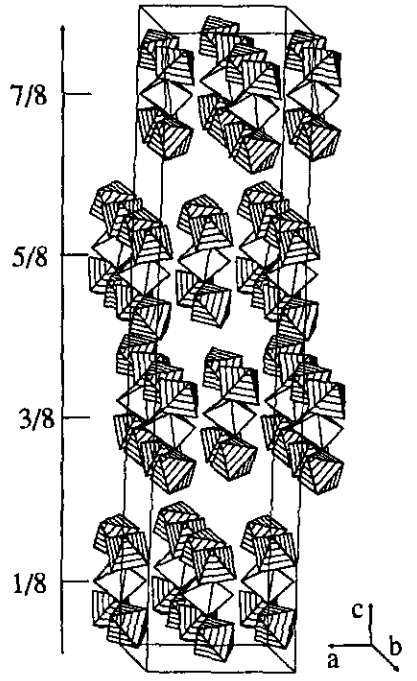

FIG. 1. Perspective view of $[Fe_5F_{26}]^{11-}$ octahedra pentamers in $Na_7Sr_2Fe_7F_{32}$ (shaded octahedra $[Fe(3)F_6]$; unshaded octahedra $[Fe(1)F_6]$).

(1.285 Å) as well as the Fe–F distances observed in most ferric fluorides (15). As usual, the longer Fe–F distances are relative to the shared fluorine atoms; however, in the $[Fe(1)F_6]$ octahedron, the distances between iron and

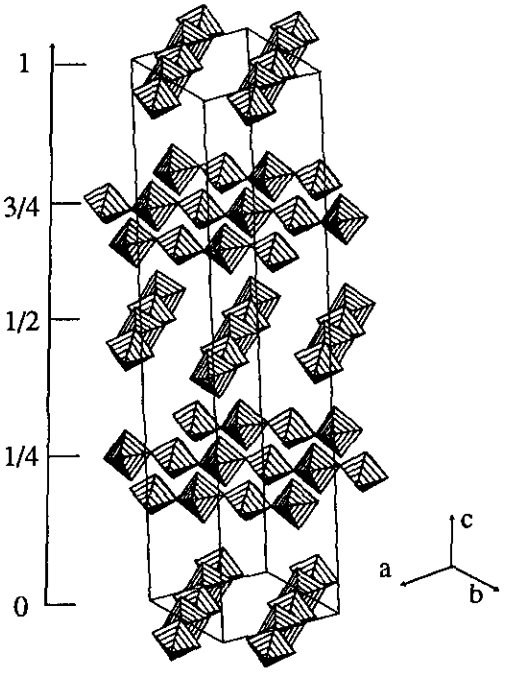

FIG. 2. Perspective view of $[FeF_5]_n^{2n-}$ chains in $Na_7Sr_2Fe_7F_{32}$.

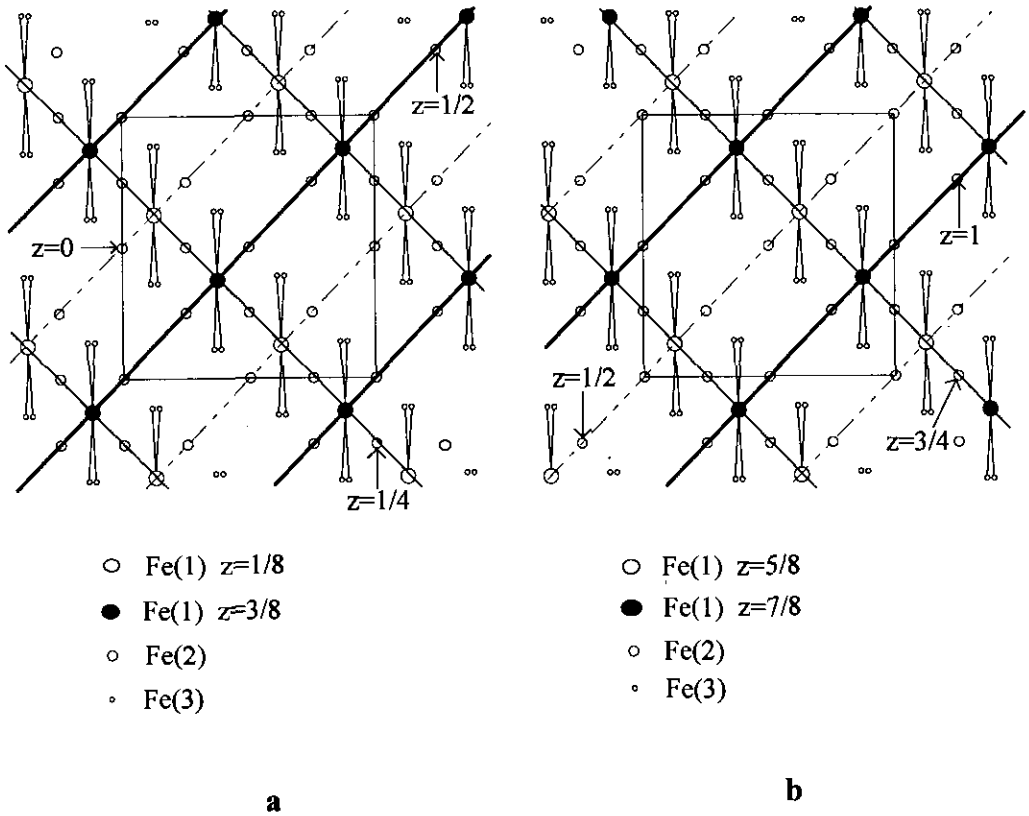

FIG. 3. (001) projection of the iron cations network: (a) $0 \leq z \leq 0.5$, (b) $0.5 \leq z \leq 1$. The different lines schematize the Fe(2) chain direction and the z coordinate of Fe(2) iron cations in each chain is indicated.

shared fluorine atoms (Fe(1)–F(7) = 1.918 Å) are found to be shorter. One can note that the distances between iron and terminal fluorine atoms (Fe(1)–F(9) = 1.838 Å) are also observed to be very short; such values have already been encountered in AMF_4 compounds (15) for the $Fe–F_{terminal}$ and seem to be a peculiar feature of the $M–F_{terminal}$ distance in the pentamers of the $Na_3Sr_4M_5F_{26}$ phases ($M = Al^{3+}, Cr^{3+}$). These short distances must be linked, in our case, to the high thermal motion of F(7) and F(9) fluorine atoms but attempts to delocalize the F(9) atom on the 32*h* site (occupation ratio, 1/2) in the *Fddd* space group and in subgroups of lower symmetry did not make it possible to improve the reliability, the Fe–F distances, and (or) the thermal motions.

The sodium (Na(1), Na(2), Na(3)) and strontium (Sr(1)) polyhedra also give rise to a three-dimensional network. Figure 5 shows how the $[Na(1)F_8]$ and $[Na(2)F_8]$ polyhedra build up (a, b) planes by sharing corners and edges at z = 1/8, 3/8, 5/8, and 7/8 (the same levels as the pentamers the central octahedron $[Fe(1)F_6]$). The $[Na(1)F_8]$ polyhedron can be seen as a distorted cube and the $[Na(2)F_8]$ polyhedron as a distorted triangulated dodecahedron called a bisdisphenoid. The regular bisdisphenoid consists of two interpenetrating tetrahedra (disphenoids), one elongated and the other flattened; in the present study the second is a square plane. The $[Sr(1)F_{10}]$ polyhedra build up infinite chains by sharing faces and are connected to chains of $[Fe(2)F_6]$ octahedra by vertices to form (a, b) planes at z = 0, 1/4, 1/2, and 3/4 (Fig. 6). Between these planes and chains are inserted the Na(3) polyhedra (flattened pentagonal bipyramid) to build up the three-dimensional

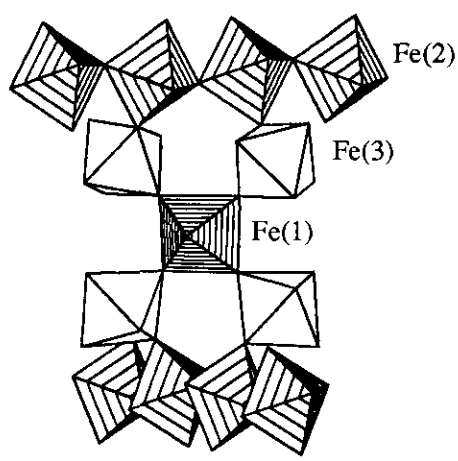

FIG. 4. Connection mode between pentamers and chains.

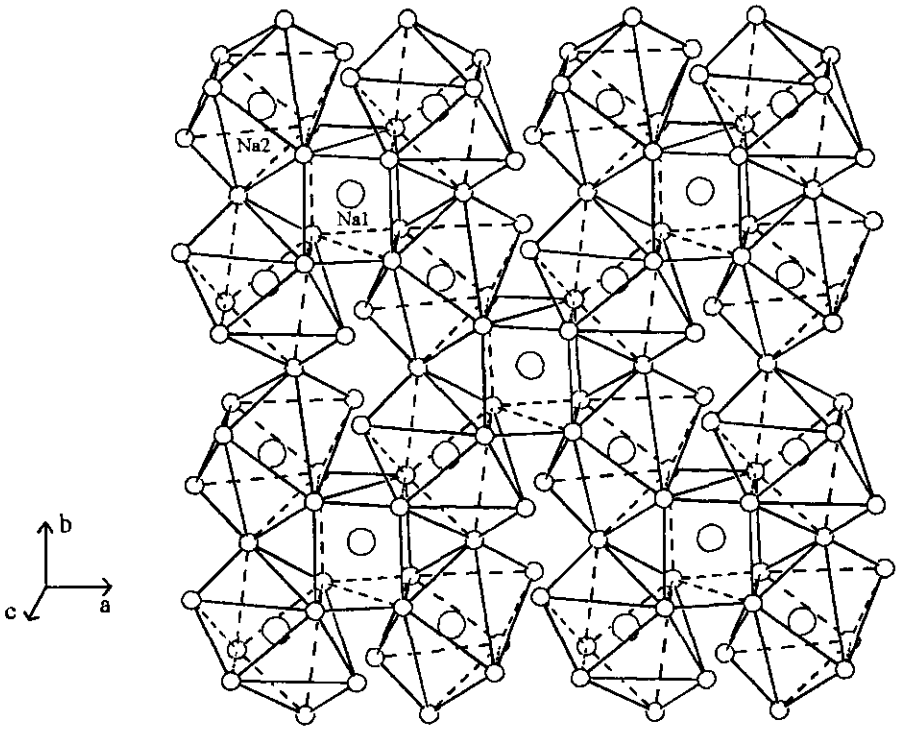

FIG. 5. Perspective view of Na(1), Na(2) polyhedra plane at $0 < z < 1/4$.

network; connections Sr(1)–Na(3) and Na(3)–Na(2) are shown in Fig. 7. The Na(3) polyhedron exhibits two short distances (≈2.20 Å) on either side of the pseudo-pentagonal plane; this situation has been encountered in most of the $Na_2MM'F_7$ weberites (16–21) where sodium atoms adopt similar seven- or eightfold coordinations (pentagonal or hexagonal bipyramids).

Structural correlations can be made with the $Na_3Sr_4Al_5F_{26}$ structure, where the same arrangement of Na polyhedra and pentamers is encountered as illustrated in Fig. 8. Indeed, the a and b cell parameters of these phases are rather close: $a_{Al} = b_{Al} = 10.26$ Å, $a_{Fe} = 10.37$ Å, $b_{Fe} = 10.80$ Å. On the other hand, the c cell parameters are strongly different: $c_{Al} = 18.37$ Å and $c/2_{Fe} = 22.49$ Å. This difference can be explained by the insertion of $[Sr_2Fe_2F_{14}]^-_{(\text{phase F32})}$ planes between $[Na_7M_5F_{26}]^{4-}$ blocks with connection by vertex in which the $Sr_{(\text{phase F26})}$ atoms are replaced by $Na(3)_{(\text{phase F32})}$ atoms (see Fig. 9).

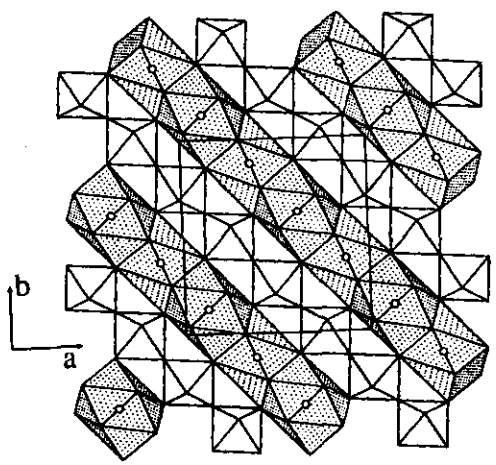

FIG. 6. (001) projection of $[Sr(1)F_{10}]$ polyhedra chains and $[Fe(2)F_5]^{2n-}_n$ chains in the same plane (z coordinate of cations ≈1/4).

It may be remarked that the radii of Sr^{2+} and F^- ions are rather close, and the replacement of Sr^{2+} by F^- creates a new octahedral site which can be occupied by a trivalent iron cation (⟨Fe–F⟩ = 1.908 Å). Thus, the $[FeF_5]_n$ infinite chains could be replaced by $[FeF_4]_n$ octahedra planes inserted between the pentamers as illustrated in Fig. 10. This hypothetical compound would have the formula $Na_7Fe_9F_{34}$. Unfortunately, this composition led to the solid state synthesis of $NaFeF_4$.

MAGNETIC BEHAVIOR

Magnetic Study

The inverse of susceptibility and magnetization curves versus temperature are presented in Figs. 11 and 12, whereas the main magnetic results are reported in Table 4. The shape of the χ^{-1} curve is rather complex, and four ranges of temperature can be considered. At high temperature ($180 < T < 290$ K), the linear decrease is in agreement with a Curie–Weiss law and leads to a C_M value not far from the calculated one; the Curie paramagnetic

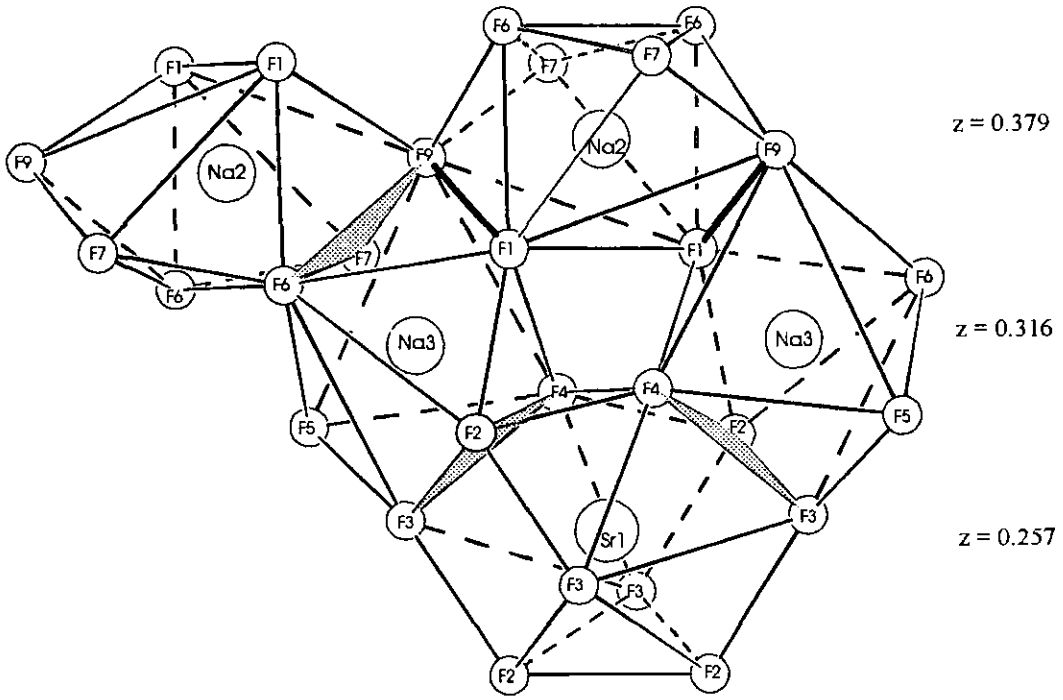

FIG. 7. Connection mode of Sr(1), Na(2), and Na(3) polyhedra.

temperature (−94 K) indicates the presence of predominant antiferromagnetic interactions according to the Kanamori–Goodenough rules (22, 23) for d^5–d^5 octahedra sharing vertices. Between 70 and 180 K the inverse susceptibility drops, as commonly observed for a ferrimagnetic compound. Then the second linear evolution clearly evidenced over the temperature range 30–70 K can be associated with a paramagnetic Curie temperature estimated to −4 K: the increase of θ'_P value also suggests the presence of ferromagnetic interactions. The last range of temperature ($T < 30$ K) consists of a rather flat domain (see insert in Fig. 11) without appearance of a critical temperature. The magnetization curve exhibits a large decrease till about 30 K, which can be considered as the critical temperature, and then the induced signal slowly vanishes at about 110 K (one can note that no remanent magnetization has been observed). Moreover, at low temperature, the magnetization becomes saturated toward a value close to 10 μ_B/mol (9.2 μ_B/mol at 2 K with $H = 10$ kOe). All these observations indicate that there probably exists a continuous dynamical reorientation of the iron spins in the structure due to a competition between antiferromagnetic and ferromagnetic interactions.

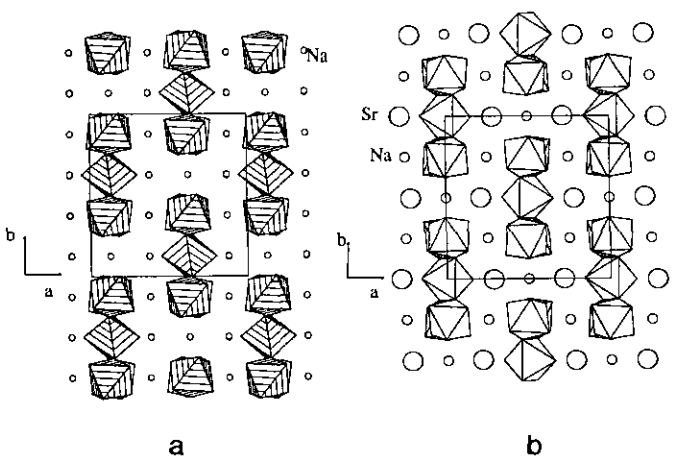

FIG. 8. Arrangement of pentamers and Na and Sr atoms in (a) $Na_7Sr_2Fe_7F_{32}$ ($0 < z < 1/4$) and (b) $Na_3Sr_4Al_5F_{26}$ ($-1/4 < z < 1/4$).

Let us now consider the superexchange angles between iron sites as given in Table 3. According to the prediction rules, magnetic interactions can be classified as follows, from strongest to weakest: the strongest within the pentamers ($Fe(1)_{(site\ 8b)}$–Fe–$Fe(3)_{(site\ 32h)}$), then the next strongest in the octahedra chains ($Fe(2)_{(site\ 16d)}$–Fe–Fe(2)), and finally the weakest between chains and pentamers (superexchange angle of 137°). From this analysis, an explanation of the second linear domain can be given. Indeed, for $30 < T < 70$ K, the antiferromagnetic couplings within the pentamer could lead to a cluster-like group with $S' = 15/2$. Then considering a paramagnetic behavior of these "clusters" with the remaining iron in the chains (two irons with $S = 5/2$), one can calculate a Curie constant $C'_M = [2 \times 35 + 4\ S'(S'' + 1)]/8 = 40.6$, close to the observed value of 37.5. Taking into account the preliminary Mössbauer results (3D magnetic ordering below

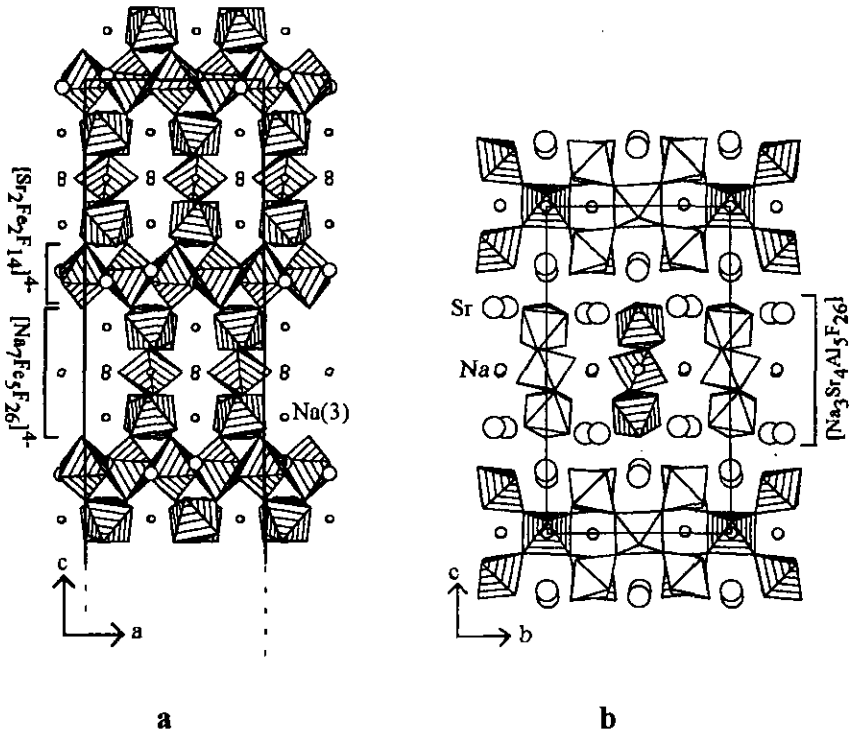

FIG. 9. (a) (010) projection of $Na_7Sr_2Fe_7F_{32}$ part and (b) (100) projection of $Na_3Sr_4Al_5F_{26}$.

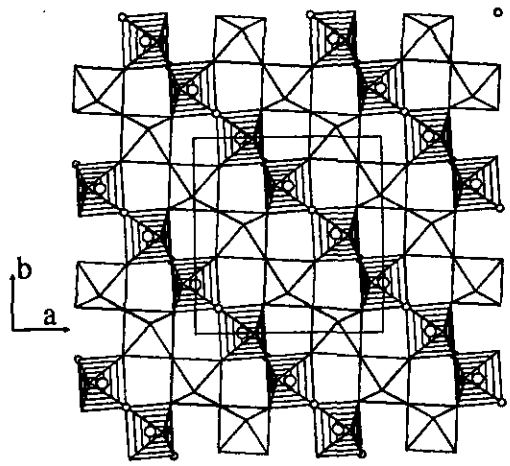

FIG. 10. The effect of replacing Sr^{2+} by F^- (small circles) creates new octahedral sites (large circles) (compare with Fig. 6); new iron octahedra are shaded.

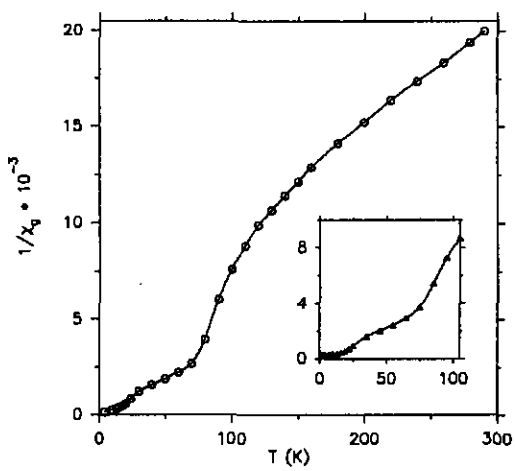

FIG. 11. Thermal evolution of the inverse magnetic susceptibility for $Na_7Sr_2Fe_7F_{32}$.

TABLE 4
Magnetic Data of $Na_7Sr_2Fe_7F_{32}$

$C_{M\ theo}$	$C_{M\ exp}$	θ_P (K)	$C'_{M\ exp}$	θ'_P (K)	$\sigma_S{}^a$ (μ_B/mol)	T_C (K)
30.6	25.8	-94 ± 5	37.5	-4 ± 2	9.2	≈30

[a] At 2 K with an applied field of 10 kOe.

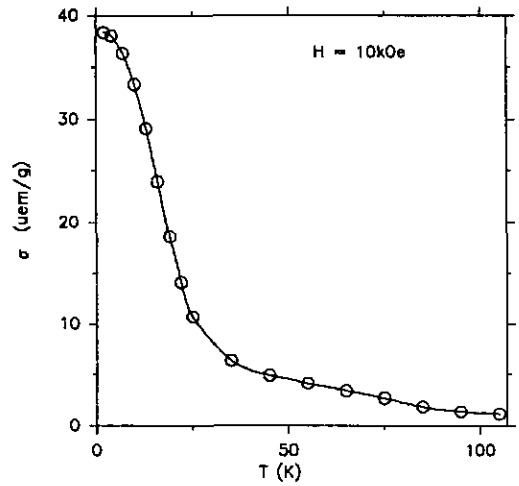

FIG. 12. Magnetization curve plotted as a function of temperature for $Na_7Sr_2Fe_7F_{32}$.

40 K) and saturation values (σ_S, see Table 4), it can be easily concluded that the magnetic coupling within the octahedra chains should be ferromagnetic. Such a situation, if realistic, results from the competition between antiferromagnetic and ferromagnetic interactions. Indeed, this can be related to the cationic topology of the structure, which involves a five-membered ring of octahedra (Fe(1), 2 × Fe(3), and 2 × Fe(2); see Fig. 4) favoring the magnetic frustration.

Mössbauer Study

The paramagnetic spectra are illustrated in Fig. 13, whereas the refined values of the hyperfine parameters are listed in Table 5. Because of the shape of these spectra,

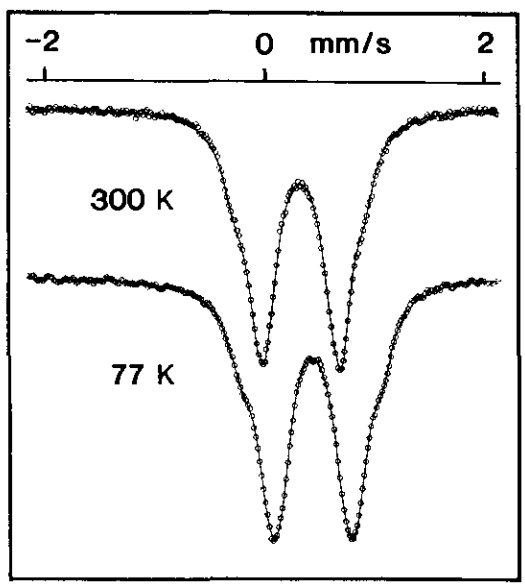

FIG. 13. Paramagnetic Mössbauer spectra recorded at given temperatures on $Na_7Sr_2Fe_7F_{32}$.

TABLE 5
Hyperfine Characteristics in the Paramagnetic Range on $Na_7Sr_2Fe_7F_{32}$

	δ^a (mm · sec^{-1}) (±0.01)	Γ^b (mm · sec^{-1}) (±0.01)	QS^c (mm · sec^{-1}) (±0.02)	Percentage^d (±2)
300 K	0.45	0.27	0.74	54
	0.46	0.28	0.59	31
	0.45	0.26	1.18	15
77 K	0.55	0.31	0.78	59
	0.55	0.25	0.57	27
	0.54	0.25	1.29	14
55 K	0.55	0.32	0.80	55
	0.55	0.28	0.54	29
	0.54	0.32	1.26	16

[a] Isomer shift value given relative to metallic iron at 300 K.
[b] Linewidth at half-height.
[c] Quadrupolar shift.
[d] The expected populations are 57.1, 28.6, and 14.3 for the iron sites Fe(3), Fe(2), and Fe(1) noted 32*h*, 16*d*, and 8*b*, respectively.

a first description leads to the existence of two quadrupolar components. The room temperature spectrum is well reproduced with only two doublets, whereas at least three quadrupolar components are required at the lower temperatures 55 and 77 K. Such an analysis is in agreement with the existence of the three crystallographic iron sites labeled Fe(1), Fe(2), and Fe(3), as discussed in the above section. The 300 K Mössbauer spectrum was then reanalyzed with three components, keeping all the parameters free during the fit. From the hyperfine data, one can conclude that (i) the relative proportions of the three Mössbauer contributions are close to those expected from the crystallographic structure, (ii) the isomer shift values are typical of high-spin-state sixfold-coordinated trivalent iron ions, and (iii) the quadrupole splitting values qualitatively reflect the different neighboring of the iron ions.

Below 40 K, the Mössbauer spectra exhibit a highly complex Zeeman hyperfine structure (see Fig. 14), consistent with a magnetically ordered phase whose parameters are listed in Table 6. At liquid helium temperature, three magnetic sextets are clearly evidenced and their relative proportions agree well with those observed in the paramagnetic range and with those expected from the crystallographic structure. When the temperature increases, the hyperfine structure becomes more complex: one can distinguish two sextets with rather sharp lines and a third magnetic component with broad lines. Thus, the spectra were fitted by considering two independent sextets Fe(1) and Fe(2) and a continuous and discrete distribution of static hyperfine field to take into account the broadening of the lines of the Fe(3) component. Such a broadening

is characteristic of a dynamical behavior of the spins (24). Indeed, accounting for the previous magnetic observations, it can be suggested that the Fe(3) magnetic moment strongly fluctuates, as an "idle spin" (25): this phenomenon probably originates from a weak magnetic coupling to the net magnetization, due to a competition of interactions. From this preliminary study, it is observed that

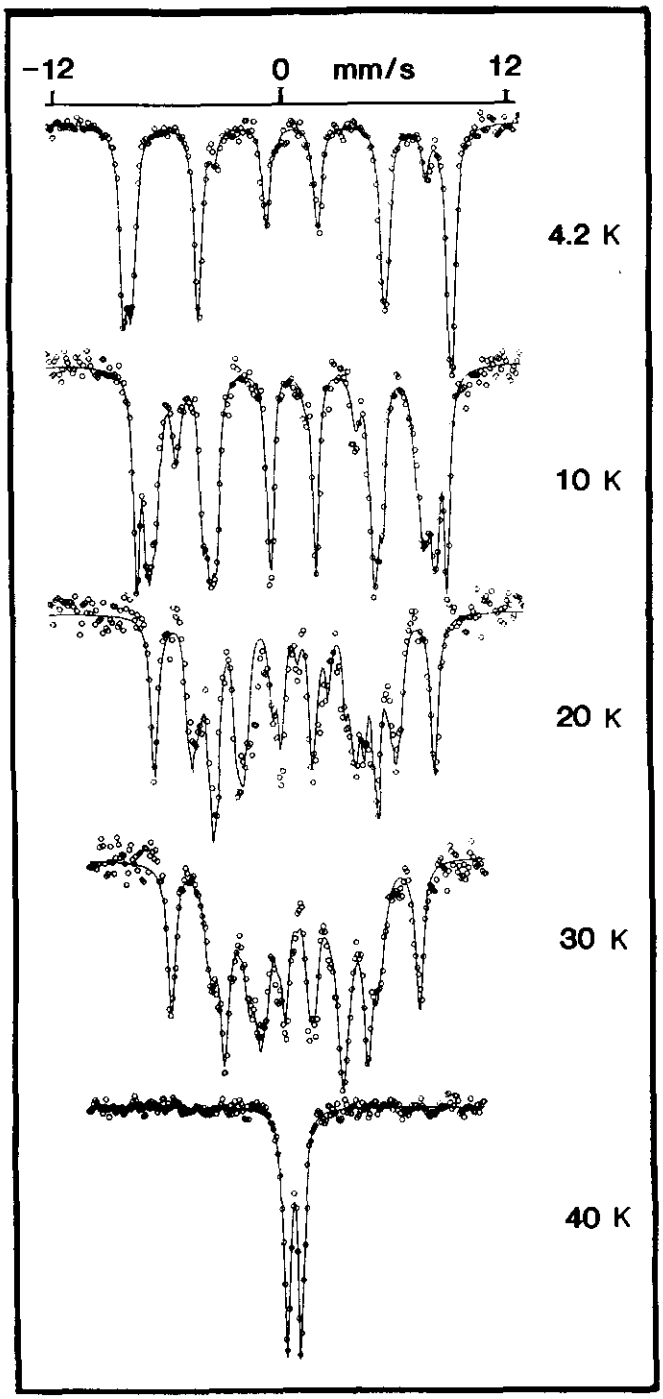

FIG. 14. Magnetic Mössbauer spectra recorded at given temperatures on $Na_7Sr_2Fe_7F_{32}$.

TABLE 6
Hyperfine Characteristics in the Magnetically Ordered Phase on $Na_7Sr_2Fe_7F_{32}$

	δ^a (mm · sec^{-1}) (±0.02)	Γ^b (mm · sec^{-1}) (±0.02)	$2\varepsilon^c$ (mm · sec^{-1}) (±0.02)	$B_{hf}{}^d$ (T) (±1.0)	Percentage^d (±2)
4.2 K	0.54	0.44	−0.21	55.0	55
	0.56	0.42	−0.05	53.1	31
	0.51	0.45	−0.99	48.6	14
10 K	0.55^e	0.30^f	−0.11^e	46.5^e	54
	0.56	0.38	−0.07	51.8	31
	0.52	0.44	0.57	40.0	15
20 K	0.55^e	0.32^f	−0.13^e	24.2^e	53
	0.55	0.48	0.01	46.7	32
	0.51	0.36	0.61	24.8	17
30 K	0.57^e	0.40^f	−0.13^e	20.8^e	56
	0.57	0.49	−0.07	41.5	29
	0.56	0.46	0.60	13.8	15

[a] Isomer shift value given relative to metallic iron at 300 K.
[b] Linewidth at half-height.
[c] Quadrupolar shift.
[d] Hyperfine field.
[e] Mean value.
[f] Fixed value during fit.

the temperature dependences of the three hyperfine fields exhibit a cusp around $T = 20$ K, in addition to different thermal evolutions. Further Mössbauer experiments are in progress in order to elucidate the temperature dependence of the magnetic behavior, in connection with the magnetic measurements.

CONCLUSION

The original structure of $Na_7Sr_2Fe_7F_{32}$ seems very interesting from a magnetic point of view. More work should be devoted to this topic. In this research (i) further Mössbauer experiments are being performed in order to specify the nature of the cusp revealed by the $H_{eff} = F(T)$ curves, (ii) in-field Mössbauer spectra are planned to follow the evolution of the magnetic structure, and (iii) neutron diffraction experiments are in preparation.

ACKNOWLEDGMENTS

The authors are grateful to Dr. R. Retoux (University of Le Mans) for his help in X-ray data collection and to Dr. P. Crespo (Instituto de Magnetismo Aplicado, Madrid) for performing SQUID measurements.

REFERENCES

1. G. Courbion, Thesis. University of Le Mans, 1979.
2. J. Nouet, C. Jacoboni, G. Ferey, J. Y. Gerard, and R. De Pape, *J. Solid State Chem.* **8**, 94 (1971).

3. A. Hemon and G. Courbion, *J. Solid State Chem.* **81,** 293 (1989).
4. A. Hemon, A. Le Bail, and G. Courbion, *J. Solid State Chem.* **81,** 299 (1989).
5. A. Hemon and G. Courbion, *J. Solid State Chem.* **87,** 344 (1989).
6. A. Hemon, A. Le Bail, and G. Courbion, *Eur. J. Solid State Inorg. Chem.* **27,** 905 (1990).
7. A. Hemon and G. Courbion, *Eur. J. Solid State Inorg. Chem.* **29,** 519 (1992).
8. A. Hemon and G. Courbion, *J. Solid State Chem.* **98,** 358 (1992).
9. A. Hemon, J. M. Greneche, and G. Courbion, to be published.
10. A. Le Bail, *J. Solid State Chem.* **83,** 267 (1989).
11. "International Tables for X-ray Crystallography," Vol. IV. Kynoch Press, Birmingham, 1968.
12. G. M. Sheldrick, *in* "Crystallographic Computing 3" (G. M. Sheldrick, C. Kruger, and R. Goddard, Eds.), p. 175. Oxford Univ. Press, London/New York, 1985.
13. G. Sheldrick, "SHELX-76: A Program for Crystal Structure Determination," University of Cambridge, 1976.
14. R. D. Shannon, *Acta Crystallogr. Sect. A* **32,** 751 (1976).
15. M. Leblanc, J. Pannetier, G. Ferey, and R. De Pape, *Rev. Chim. Miner.* **22,** 107 (1985).
16. G. Courbion, G. Ferey, H. Holler, and D. Babel, *Eur. J. Solid State Inorg. Chem.* **25,** 435 (1988).
17. O. V. Yakubovich, V. S. Urusov, G. Frenzen, W. Massa, and D. Babel, *Eur. J. Solid State Inorg. Chem.* **27,** 467 (1990).
18. M. Welsch and D. Babel, *Z. Naturforsch. B* **47,** 685 (1992).
19. P. Gravereau, A. Boireau, J. M. Dance, L. Trut, and A. Tressaud, *Acta Crystallogr. Sect. C* **48,** 2108 (1992).
20. G. Frenzen, W. Massa, D. Babel, N. Ruchaud, J. Grannec, A. Tressaud, and P. Hagenmuller, *J. Solid State Chem.* **98,** 121 (1992).
21. W. Verscharen and D. Babel, *J. Solid State Chem.* **24,** 405 (1978).
22. J. Kanamori, *J. Phys. Chem. Solids* **10,** 87 (1959).
23. J. B. Goodenough, "Magnetism and Chemical Bond." Wiley–Interscience, New York, 1963.
24. A. P. Murani, *J. Magn. Magn. Mater.* **5,** 95 (1977).
25. G. Courbion, R. De Pape, J. Teillet, F. Varret, and J. Pannetier, *J. Magn. Magn. Mater.* **42,** 217 (1984).